EPJ Web of Conferences **20**, 05001 (2012)
DOI: 10.1051/epjconf/20122005001

Experimental plan of Σp scatterings at J-PARC

K. Miwa[a], R. Honda, Y. Matsumoto, H. Kanda, H. Tamura, M. Ieiri*
and J-PARC P40 collaboration

Department of physics, Tohoku university,
High Energy Accelerator Research Organization (KEK)*

Abstract. In order to test theoretical frameworks of the baryon-baryon interactions and to confirm the "Pauli effect between quarks" for the first time, we propose an experiment to measure low-energy hyperon proton scattering cross sections in the following channels with high statistics, 1. $\Sigma^- p$ elastic scattering, 2. $\Sigma^- p \to \Lambda n$ inelastic scattering, 3. $\Sigma^+ p$ elastic scattering. According to theoretical models based on quark-gluon picture for the short range part of the baryon-baryon interactions, the $\Sigma^+ p$ channel is expected to have an extremely repulsive core due to the Pauli effect between quarks, which leads a $\Sigma^+ p$ cross section twice as large as that predicted by conventional meson exchange models with a phenomenologically treated short range repulsive core. In addition, measurement of the $\Sigma^- p$ channel where the quark Pauli effect is not effective is also necessary to test the present theoretical models based on meson exchange picture with the flavor SU(3) symmetry. Thus this experiment will provide essential data to test the frameworks of the theoretical models of the baryon-baryon interactions and to investigate the nature of the repulsive core which has not been understood yet.
In order to overcome the experimental difficulties in measuring low-energy hyperon proton scattering, we will use a new experimental technique in which a liquid H_2 target is used as hyperon production and hyperon scattering targets with a detector system surrounding the LH_2 target for detection of a scattered proton and a decay product from a hyperon. The hyperon scattering event is kinematically identified. Because imaging detectors used in past experiments are not employed, high intensity π beam can be used, allowing us to take high statistics data of 100 times more than the previous experiments.
We have proposed an experiment of Σp scattering at the K1.8 beam line by utilizing the K1.8 beam line spectrometer and the SKS spectrometer. A high intensity π beams of 2×10^7/spill at 1.32 GeV/c and 1.42 GeV/c for the Σ^- and Σ^+ productions, respectively, are used to produce as many hyperon beam as possible. With 16×10^6 Σ^- beam and 55×10^6 Σ^+ beam around 500 MeV/c which are tagged by the spectrometers, we will detect ~10,000 $\Sigma^- p$ and $\Sigma^+ p$ scattering events and ~6,000 $\Sigma^- p \to \Lambda n$ inelastic reaction events in 60 days beam time in total.
In this proceedings, we will present the experimental plan of the scattering experiment and results of the detailed simulation studies.

1 Introduction

The nuclear force is one of the most important phenomena which form all the "matter" in nature. However, our understanding of the nuclear force is quite unsatisfactory yet. In view of the current nuclear physics, understanding low energy interactions between hadrons based on QCD is an important problem to be solved. The nuclear force has been extensively studied experimentally by pp and pn scatterings, and its nature is understood well by meson exchange models in a long range attractive region of more than 1 fm. In the short range region, a strongly repulsive core exists and the miraculous

[a] e-mail: miwa9@lambda.phys.tohoku.ac.jp

S	$B_8B_8(I)$	$P = +1$ (symmetric) ^1E or ^3O	$P = -1$ (antisymmetric) ^3E or ^1O
0	$NN(I = 0)$	–	(10^*)
0	$NN(I = 1)$	(27)	–
	ΛN	$\frac{1}{\sqrt{10}}[(8s) + 3(27)]$	$\frac{1}{\sqrt{2}}[-(8a) + (10^*)]$
-1	$\Sigma N(I = 1/2)$	$\frac{1}{\sqrt{10}}[3(8s) - (27)]$	$\frac{1}{\sqrt{2}}[(8a) + (10^*)]$
	$\Sigma N(I = 3/2)$	(27)	(10)

Table 1. The relationship between the isospin basis and the flavor-SU(3) basis for the B_8B_8 systems. The heading P denotes the flavor-exchange symmetry, S the strangeness, and I the isospin.

balance between the long-range attraction and the short-range repulsion plays essential roles in the formation of the nucleus. However the nature of the short range region where two nucleons overlap is not understood; it is treated phenomenologically in conventional meson exchange models. In this region, it is expected that dynamics of quarks and gluons, the constituents of the nucleon, play an important role, and introducing a new flavor of quarks, a strangeness quark, will provide a clue to approach this problem. Thus, in order to understand the nuclear force, it is crucially important to investigate the generalized baryon-baryon (B_8B_8) interactions including the hyperon nucleon (YN) and the hyperon hyperon (YY) sectors. The theoretical studies of the B_8B_8 interactions have been developed by two different types of theoretical models, one is the one boson exchange model such as Nijmegen OBEP model based on meson exchange picture, and the other is quark based approaches such as Quark Cluster Model (QCM).

The Nijmegen group developed one boson exchange (OBE) models that extend nuclear force to baryon-baryon interactions based on flavor SU(3) symmetry and the phenomenological core potential[1].

Many efforts have been also devoted to understand the B_8B_8 interactions based on the QCD. A direct derivation of these interactions from QCD involves tremendous difficulties, such as the quark confinement and multi-gluon effects in the low energy phenomena. The Quark Cluster Model (QCM) has been developed as a QCD-inspired model which assumes constituent quarks with the color degree of freedom in a confinement potential and takes into account the effect of one gluon exchange between them. In this model, the short range parts of the baryon-baryon interactions are calculated using the resonating group method, where color magnetic interaction from one gluon exchange and the quark Pauli effect are found to play essential roles and the nature of the NN repulsive core is naturally derived[2]. In addition, Kyoto group proposed baryon-baryon interaction models which use the Quark Cluster Model for the short range part and the meson exchange picture in the long range part[3] as a realistic interaction for calculations of YN scattering cross sections and hypernuclear structure.

Recently, a new method to extract the B_8B_8 potentials in the coordinate space from lattice QCD simulations has been proposed and applied to the NN system, and also to YN systems. The six independent B_8B_8 potentials (27, 10^*, 10, 8s, 8a, 1 where 27 and 10^* multiplet is the same with $NN(I = 1)$ and $NN(I = 0)$, respectively)for S-wave in the flavor SU(3) limit were calculated by a lattice QCD simulation [5]. The newly appeared interactions (10, 8s, 8a, 1) are predicted to show an interesting characteristics which are different from the NN interaction especially in the short range region. The (8s) component is completely Pauli forbidden for the most compact $(0S)^6$ configuration, where all constituent quarks occupy the 0S state, and is characterized by the strong repulsion originating from the quark Pauli principle. The (10) state is almost Pauli forbidden, and thus the interaction is also strongly repulsive. On the other hand, the (8a) state turns out to have a very weak interaction. The (1) component in the H-particle channel is attractive because of the color-magnetic interaction. The features of the calculated potentials completely agree with the Quark Cluster Model prediction. This agreement suggests that the quark Pauli blocking plays an essential role for the repulsive core in B_8B_8 systems as originally proposed in [2].

In order to investigate the B_8B_8 interactions, the hyperon proton scattering experiment is the most powerful method because it enables us to give information on wider flavor channels. Table 1 shows the relationship between the isospin basis and the flavor-SU(3) basis for the B_8B_8 interaction. In order

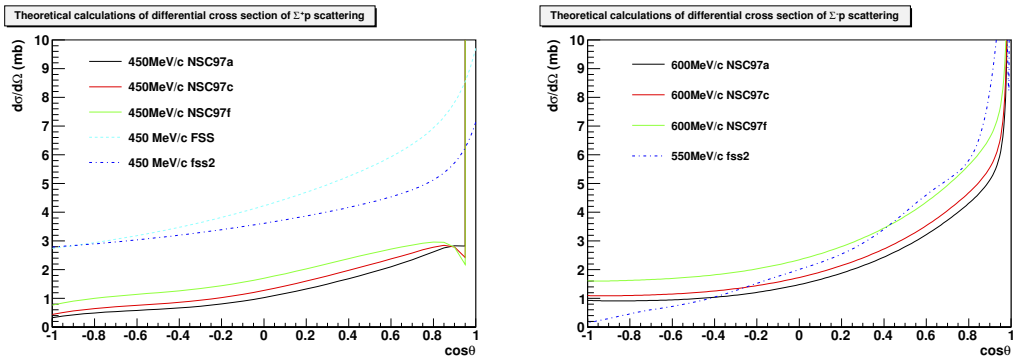

Fig. 1. Theoretical predictions by the OBEP (Nijmegen Soft Core) models and the quark cluster (RGM FSS) models for $\Sigma^+ p$ and $\Sigma^- p$ elastic scatterings. The difference of the differential cross section of $\Sigma^+ p$ channel is originated from a repulsive core due to the quark Pauli effect.

to study the framework of $B_8 B_8$ interactions and to investigate the nature of repulsive core, the ΣN system plays an important role. The ΣN interaction is expected to be quite dependent on the configuration of the isospin and spin. Especially, the $\Sigma^+ p$ channel is expected to be very repulsive due to the (10) configuration which is almost Pauli forbidden state. As shown in Table1, the $\Sigma^+ p$ channel is simply described by two multiplets. The spin singlet state is described by the (27) configuration which is the same multiplet as the $NN(I = 1)$ interaction. The spin triplet state is represented by the (10) configuration which is expected to be quite repulsive due to the almost Pauli forbidden state. Because the contribution of the triplet state is 3 times larger than the singlet state, the $\Sigma^+ p$ interaction is dominated by the Pauli forbidden state. In the Quark Cluster Model, this strongly repulsive force is derived naturally as the effect of Pauli principle between quarks, while, in the OBE model, such a strongly repulsive force is not obtained. These different strengths of the repulsive forces give sizable differences between the cross sections calculated by these theoretical models as shown in left figure of Fig. 1.

On the other hand, in the $\Sigma^- p$ channel, there is no large difference between cross sections by these two models as shown in right figure of Fig. 1, although the $\Sigma^- p$ channel in $(I = 1/2, S(spin) = 0)$ includes the (8s) configuration which is completely Pauli forbidden state. It means that the contribution of boson exchange is expected to be large in both theoretical calculations. Therefore measurement of the differential cross section of the $\Sigma^- p$ $(\rightarrow \Lambda n)$ channel provides a decisive test for the theoretical models based on meson exchange picture with the flavor SU(3) symmetry. Once the meson exchange theoretical model is confirmed by the $\Sigma^- p$ data, the $\Sigma^+ p$ data allow us to investigate the quark Pauli effect in the short range by comparing the data with theoretical predictions by QCM and OBEP.

Therefore it is essential to measure the scattering data of the $\Sigma^\pm p$ and $\Sigma^- p \rightarrow \Lambda n$ reactions to develop the whole picture of the $B_8 B_8$ interaction.

2 Experimental goal

We propose an experiment to measure the $\Sigma^- p$ and the $\Sigma^+ p$ elastic scattering cross sections and the $\Sigma^- p \rightarrow \Lambda n$ reaction cross section with 100 times larger statistics than the previous experiments[6][7][8]. From the experience of the past experiments, we designed new experimental setup and conditions by considering the following points:

- High rate meson beam should be handled to produce intense hyperon beam.
- Liquid hydrogen should be used as hyperon production and hyperon-proton scattering targets to be free from the unwanted background such as a quasi-free scattering on other nuclei.
- A sophisticated trigger system should be developed for the efficient selection of the hyperon production and the hyperon scattering events under the high intensity meson beam.

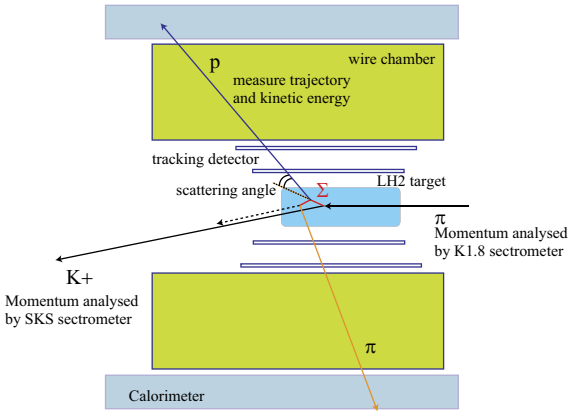

Fig. 2. Conceptual experimental setup for the YN scattering using a liquid hydrogen target and the surrounding detectors. The Σ beam is tagged by the detection of the incident π beam and the outgoing K^+ with the beam line spectrometer and the SKS spectrometer, respectively. The surrounding detector is used for the detection of the recoil proton and the decay product of the hypron. The reaction kinematics of the Σp scattering can be reconstructed from the information of the Σ beam and the recoil proton.

Fig. 2 shows the conceptual experimental setup. We use a liquid hydrogen (LH_2) target as hyperon production and hyperon-proton scattering targets. The tracking detectors are placed surrounding the LH_2 target to detect the scattered proton and the decay product from the hyperon. For the scattered proton, its trajectory and the kinetic energy are measured by the detectors surrounding the LH_2 target. Since the momentum vector of the Σ beam can be reconstructed by the beam line and the forward spectrometers, the scattering angle can be obtained by the angle defined by the Σ^- beam and the scattered proton. These three measurements, namely the Σ beam momentum, the scattering angle, and the energy of the scattered proton, combined with the use of the LH_2 target enable us to identify the scattering event. This is because the reaction is two body reaction and thus its kinematics is uniquely determined.

A high intensity π beams of 2×10^7/spill at 1.32 GeV/c and 1.42 GeV/c for the Σ^- and Σ^+ productions, respectively, are used to produce as many hyperon beam as possible. With 16×10^6 Σ^- beam and 55×10^6 Σ^+ beam around 500 MeV/c which are tagged by the spectrometers, we will detect ~10,000 $\Sigma^- p$ and $\Sigma^+ p$ scattering events and ~6,000 $\Sigma^- p \to \Lambda n$ inelastic reaction events in 60 days beam time in total. The expected results is shown in Fig. 9, 10 and 8 for the $\Sigma^- p$, $\Sigma^- p \to \Lambda n$ and $\Sigma^+ p$ channels, respectively, in Section 4.2.

As an important feature of scattering experiments, the energy dependence of the cross section is related to the shape of the potential. Especially, in order to investigate the short range repulsive core, the differential cross section of the S-wave has an essential information. In the partial wave analysis, the differential cross section is described by the following equation,

$$\frac{d\sigma}{d\Omega} = \frac{1}{k^2}\left|\sum_{l=0}^{\infty}(2l+1)e^{i\delta_l}\sin\delta_l P_l(\cos\theta)\right|^2. \quad (1)$$

Because $P_l(0)$ is 0 for odd l, the S-wave contribution is large for the differential cross section at $\theta = 90^o$. For the NN interaction, the repulsive core radius was estimated from the energy dependence of the differential cross section at $\theta = 90^o$ by R. Jastrow before the precise partial wave analysis as shown in Fig. 3. The differential cross section data were compared with calculations in which the repulsive core was represented by a hard sphere, with the radii of 0.5 and 0.6×10^{-13} cm [9]. At present the YN interactions are in a similar situation to Fig. 3 and the precise partial wave analysis is still difficult in the proposed experiment. However, the energy dependence provides quite important information and the value at $\theta = 90^o$ is directory connected to the phase shift δ_0. In Fig. 3, the sensitivity for the energy dependence of the $\Sigma^+ p$ differential cross section around 90 degree ($-0.1 < \cos(\theta) < 0.1$) in

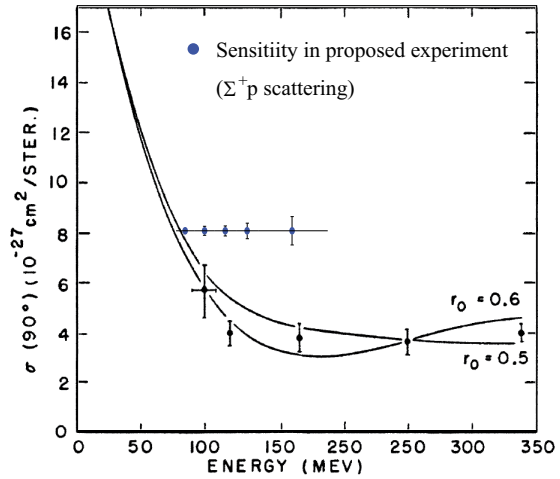

Fig. 3. First estimate of the hard core radius of the nuclear force by R. Jastrow [9]. The differential cross section of the pp scattering at 90° is shown with theoretical predictions with different core radius assumptions. The blue points show the sensitivity for the $\Sigma^+ p$ scattering, where the absolute value has no meaning.

the proposed experiment is overwritten with the pp data. Although the energy is still limited around $80 < E_{kin}$ (MeV) < 170, this will be the first data of energy dependence with enough sensitivity. For the low energy region, the bubble chamber data can be referred. The higher energy region will be obtained by changing the detection angle of the K^+ where we need the different experimental setup. By accumulating the energy dependent data, we can experimentally provide the information about the repulsive core. The proposed experiment is the 1st step toward this goal.

3 Experimental setup

For this experiment, we plan to utilize the SKS spectrometer and the K1.8 beam line spectrometer at the K1.8 beam line. In addition to the normal K1.8 experimental setup, we newly install a detector system dedicated for the proposed experiment which includes a liquid hydrogen target and the surrounding detectors of fiber tracker, drift chamber and calorimeters in order to detect the scattered proton and the charged particles from hypron decay.

3.1 Magnetic spectrometers to tag Σ beams

In order to identify the $\pi^\pm p \to K^+\Sigma^\pm$ reactions and to measure the Σ hyperon beams, the SKS spectrometer and the K1.8 beam line spectrometer are utilized. Fig. 4 shows the experimental setup of the K1.8 beam line and the SKS spectrometers. We use the π^- beam of 1.325 GeV/c for the Σ^- production and the π^+ beam of 1.419 GeV/c for the Σ^+ production, respectively, because the (π, K^+) reaction can identify the Σ production without any background. When the forward scattered K^+ is detected by the forward spectrometer, the momentum of the Σ hyperons produced by the $\pi p \to K^+\Sigma$ reaction is larger than 400 MeV/c.

In order to obtain intense Σ beams, the intensity of the incident π beam is required to be 10^7 Hz, which corresponds to 2×10^7/spill in 2 sec. extraction time during 6 sec. cycle. The spill of the current slow extraction has a spike structure where very intense beam comes instantaneously. The present beam rate is determined by this beam structure. At the K1.8 beam line, two MWPC's (BC1,2) and two MWDC's (BC3,4) are installed upstream and downstream of the beam line spectrometer magnet, respectively. These chambers are originally designed to work at 10^7 Hz beam rate. However it is

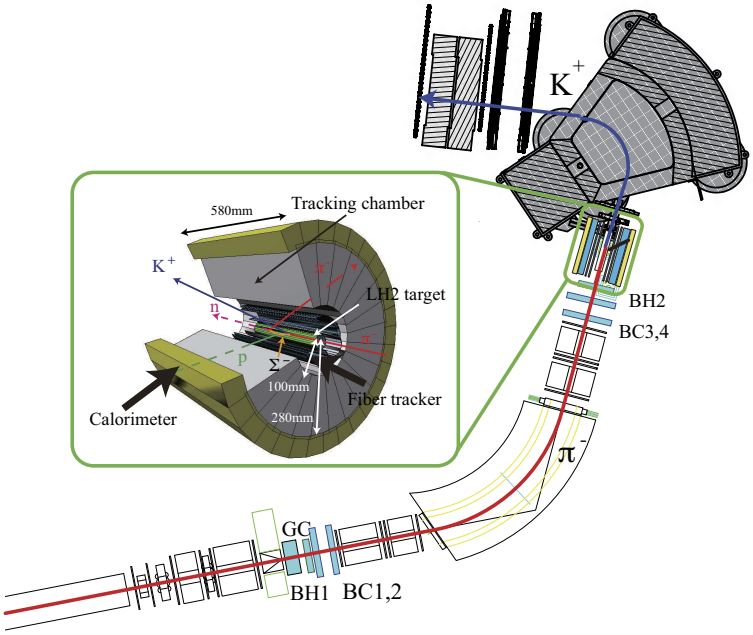

Fig. 4. Experimental setup of the K1.8 beam line. The K1.8 spectrometer and the SKS spectrometer analyze the incident π beam particle and the scattered K^+, respectively. The left figure shows a schematic view of the LH_2 and surrounding detector system. The LH_2 target is surrounded by 4 layers of fiber tracker, cylindrical drift chamber and calorimeter.

difficult to operate these chambers in the present beam condition. In these situation, in order to handle the high intensity π beam, the fiber tracker will be used, which is stable for the high intensity beam and has a better time resolution of 1 nsec. This better time resolution enables us to separate the real beam particle, which interacts at the target, from the accidental beam. The incident π beam particles are defined by the two beam hodoscopes (BH1,2) placed about 11 m apart. The electron contamination is rejected by a gas cherenkov counter placed upstream of BH1. The momenta of the incident π beam particles are analyzed by the K1.8 beam line spectrometer which consists of QQDQQ magnet system and beam line fiber trackers. The original momentum resolution of the K1.8 beam line spectrometer is 0.014 % in rms. The usage of the fiber trackers makes the resolution worse due to the multiple scattering. However, the resolution is acceptable for the proposed experiment. The readout system of the fiber tracker will be the same technology with the fiber vertex tracker which is described in the next subsection. The PPD (MPPC) and the special readout board using an ASIC (SPIROC-A) [10] for PPD are used.

Scattered K^+'s are detected with the SKS spectrometer. The magnetic field is set to 2.1 T for the $\pi^- p \rightarrow K^+\Sigma^-$ reaction with 1.3 GeV/c π^- beam. For the Σ^+ production via the $\pi^+ p \rightarrow K^+\Sigma^+$ reaction, we use 1.4 GeV/c π^+ beam, where the magnetic field is increased up to 2.4 T. The momentum of each outgoing particle is analyzed with four drift chambers (SDC1,2,3,4) located upstream and downstream of the SKS magnet. For particle identification, trigger counters (TOF, AC1·2, LC) are placed downstream of SDC4. For the identification of K^+, hits of TOF and LC and veto of AC are required.

The function of the spectrometers is to tag as many Σ beams as possible with good momentum and angular resolutions. Fig. 5 shows the expected missing mass of Σ^- and the kinematical values for the $\pi p \rightarrow K^+\Sigma$ reactions. The acceptances of the SKS for the Σ^- and Σ^+ reactions are 4.5% and 7.0%, respectively, taking into account the target position in the present experiment. The momenta of the scattered K^+ are ~0.8 GeV/c and ~0.97 GeV/c for the Σ^- and Σ^+ productions, respectively. Because the distance between the target and LC wall is ~7.2 m, the survival rates of the K^+'s are 34 % and 41

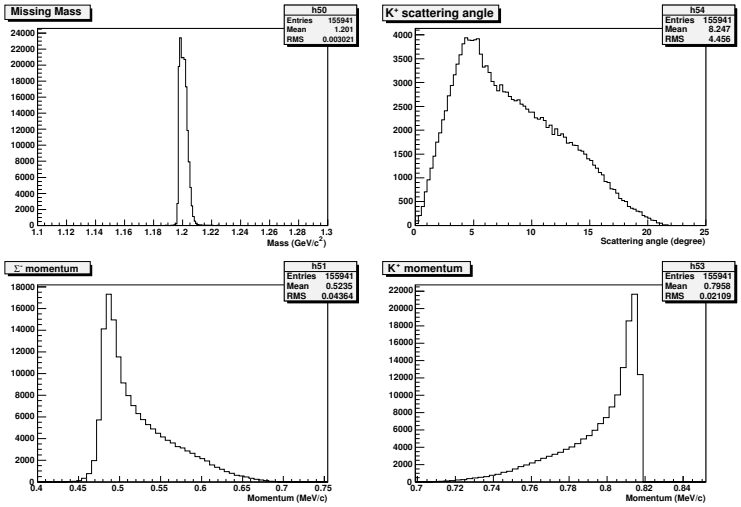

Fig. 5. Left-Top: Expected missing mass spectrum of Σ^-. Right-Top: Angular distribution of the scattered K^+. Left-Down: Σ^- momentum distribution. Right-Down: K^+ momentum distribution.

%, respectively. The Σ^- beam momentum has a peak at 0.49 GeV/c and ranges from 0.45 to 0.7 GeV/c as shown in Fig. 5. For the Σ^+, beam momentum has a peak at 0.45 GeV/c and ranges from 0.42 to 0.65 GeV/c.

3.2 Detector system to identify the Σp scattering

The enlarged figure in Fig. 4 shows a schematic view of the LH_2 target and surrounding detector system. We use a 30 cm long LH_2 target as hyperon production and hyperon proton scattering targets. The target diameter of 4∼6 cm is considered, because hyperon cannot move inside the target for a long range due to its short life time. Therefore it should be comparable with the mean path length in the hyperon beam.

The LH_2 target is surrounded from inner to outer region by a scintillation fiber tracker made from 4 layers of scintillation fiber sheet, a cylindrical drift chamber and calorimeters in order to measure the trajectories of the scattered proton and the decay products from hyperon. The energy of the proton can be measured by the calorimeter. However the detailed setup around target is still under consideration.

3.2.1 Fiber tracker for vertex reconstruction and trigger

In realizing hyperon proton scattering with high statistics, it is essential to use high intensity π or K^- beams to produce enough hyperon beams. Accordingly, the ability to separate the real scattering events from the accidental coincidence events is necessary. Because we do not use an imaging detector, the accidental coincidence events with the Σ production might cause some errors in deriving the cross section. A good time resolution of ∼1 ns to separate the accidental events is required. Therefore we will install a fiber tracker at the most inner part, which also works as a vertex tracking system. The ability to trigger by the scattering events is also essential for high statistics experiment. Using the difference of the energy deposit in the fibers of π and proton, any charged particle events or proton events can be selected on the trigger level. The fiber tracker is a three dimensional tracking detector. whose odd and even layers have a u and v configuration, respectively. The cross section of the fiber is 0.5×1 mm^2 and the total readout channel is ∼1500. The each fiber signal is detected by PPD (MPPC) with a special readout board SPIROC, which enables us to read 32 ch of MPPC serially.

The SPIROC chip is an ASIC dedicated for the multi-channel PPD readout. The SPIROC chip has 32 channel inputs of PPD and each channel has a preamplifier, slow shaper for an energy measurement, and fast shaper and discriminator for a time measurement [10]. The each discriminator output signal is sent to a FPGA control chip, then time information is obtained with a few ns resolution. By setting the threshold to the energy deposit of protons, these logic signals can also be used as a trigger.

4 Analysis of simulated data and the expected results

In order to check our experimental sensitivity, we performed a detailed Monte Carlo simulation study by generating the $16{\times}10^6$ tagged Σ^- beam and the $55{\times}10^6$ tagged Σ^+ beam which are the expected number of the Σ beams. In this section, the analysis to identify the Σp scattering and the expected results are described.

4.1 Identification of $\Sigma^- p$ elastic scattering

In this subsection, we will describe how Σp scattering events can be identified kinematically by taking $\Sigma^- p$ elastic scattering case as an example. In the Σ^- beam experiment, there are five possible reactions where a proton is emitted in coincidence with the Σ^- production: the $\Sigma^- p$ elastic scattering, Λn inelastic scattering, $\Sigma^0 n$ inelastic scattering, scattering with Σ^- decay products, namely np scattering and $\pi^- p$ scattering. In these reactions, the $\Sigma^- p$ elastic scattering can be identified by detecting the scattered proton.

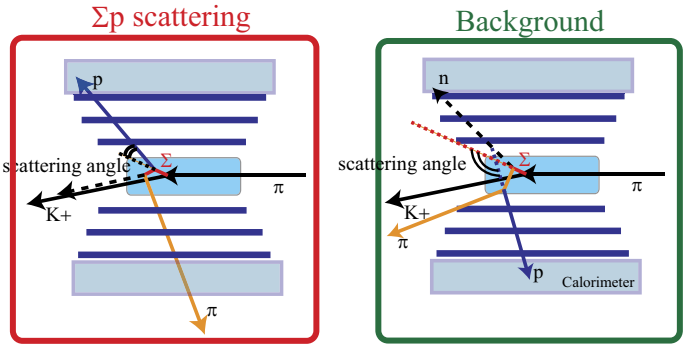

Fig. 6. Definition of the scattering angle. The angle is defined as the crossing angle between the hyperon beam track and the outgoing proton.

In the event generator in the Monte Carlo simulation, we included the background processes mentioned above. In order to identify the Σp scattering, we check the consistency between the hyperon beam momentum, the scattering angle and energy of the scattered proton. Here the scattering angle is defined by a crossing angle between the outgoing proton track and hyperon beam as shown in Fig. 6. We also used the same scattering angle for the background events. Here we define the following values,

- $E_{measure}$: measured kinetic energy of the proton by the calorimeter,
- $E_{calculate}$: calculated kinetic energy from the hyperon beam momentum and the scattering angle,
- ΔE : difference between $E_{measure}$ and $E_{calculate}$, ($\Delta E = E_{measure} - E_{calculate}$).

For the Σp scattering event, the ΔE should be zero, although the ΔE has a broad distribution for the background events. The Left-Up figure in Fig. 7 shows the ΔE distribution for the Σ^- beam events, where the peak around $\Delta E = 0$ MeV and broad structures correspond to the $\Sigma^- p$ elastic scattering

events and background events, respectively. The total cross section of the $\Sigma^- p$ elastic scattering is assumed to be 30 mb. Because the cross sections of the background reactions are also taken into account, the S/N ratio is reliable.

By detecting the π^- from the Σ^- decay, the np scattering and Λn inelastic scattering can be identified with some assumptions as explained in the previous paragraph. In the analysis, we make three ΔE (Δp for Λn reaction) distributions assuming the following three reactions, $\Sigma^- p$ elastic scattering, $\Sigma^- p \to \Lambda n$ inelastic scattering and np scattering, as shown in Fig. 7. For each assumption, there is a peak around $\Delta E = 0$ which corresponds to the assumed reaction and a broad structure due to other reactions. In order to improve the S/N ratio for the $\Sigma^- p$ and Λn reactions, the events corresponding to the np scattering are removed as a background suppression cut. The Right-Down figure in Fig. 7 shows the ΔE distribution after these background suppression cuts for $\Sigma^- p$. scattering. Although the S/N ratio is much improved, there exists the unavoidable background. When the differential cross section is derived, the contribution from the background should be subtracted.

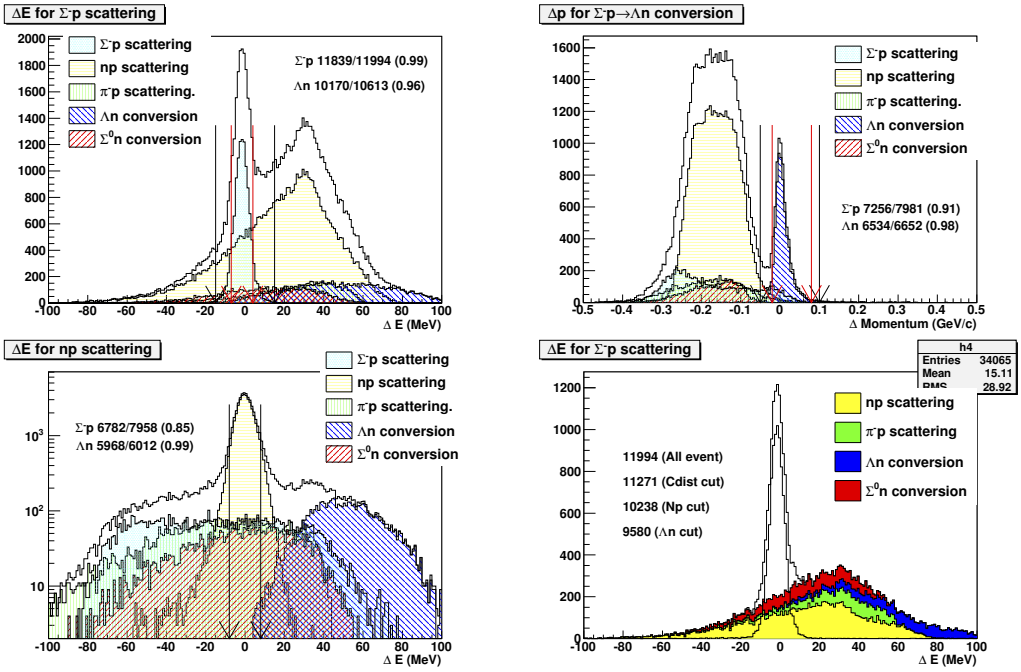

Fig. 7. ΔE distributions for $\Sigma^- p$ (Left-Up) and np scatterings (Right-Up) and Δp distribution for $\Sigma^- p \to \Lambda n$ conversion reaction (Left-Down). For the $\Sigma^- p$ scattering event, ΔE distribution makes a peak around $\Delta E = 0$, although other reactions makes the broad distributions. This relation is the same for other reactions. ΔE distributions for $\Sigma^- p$ after background suppression(Right-Down)

4.2 Expected results

The expected results studied by the simulation are shown in Fig. 8, 9 and 10 for the $\Sigma^+ p$, $\Sigma^- p$ and $\Sigma^- p \to \Lambda n$ reactions, respectively, with the two theoretical calculations, the Nijmegen model and the Quark Cluster Models. The assumed cross section in the simulation is 30 mb with a flat angular distribution. The reproduced distribution in Fig. 8, 9 and 10 shows a flat distribution with fluctuations. This shows the feasibility of the new experimental technique.

For the $\Sigma^+ p$ scattering, the Quark Cluster Model predicts a larger cross section than the OBEP model due to different treatment of the repulsive core as shown in Fig. 8. The aim of the $\Sigma^+ p$ channel is

to provide a cross section data sufficient to confirm the effect of the strongly repulsive core originating from the quark Pauli effect which appears as the difference of the differential cross section. According to our simulation, the differential cross sections, which were derived separately for the different decay modes of Σ^+, were obtained from ~2,000 and ~3,000 scattering events in the momentum region of $0.5 < p$ (GeV/c) < 0.6 for the $p\pi^0$ and $n\pi^+$ modes, respectively. Fig. 8 shows the results for the $n\pi^+$ mode. The expected result is sufficient to test the theoretical models and to give information about the nature of the repulsive core.

The two theoretical calculations show similar behavior in the $\Sigma^- p$ elastic scattering and the $\Sigma^- p \to \Lambda n$ inelastic scattering as shown in Fig. 9 and 10. In these channels, we aim to measure the angular dependence of the differential cross section with enough statistics and accuracy to test the framework of theoretical models based on meson exchange picture with the flavor SU(3) symmetry, since there is no quark Pauli effect in this channel and the other part of the interaction is essentially the same. The simulated spectra shown in Fig. 9 and 10 were obtained from ~5,000 and ~4,000 scattering events, respectively, in the momentum region of $0.45 < p$ (GeV/c)< 0.55. This data quality enables us to compare the angular dependence of the differential cross section with the theoretical models and check the theoretical framework for the first time. If theoretical models can reproduce the $\Sigma^- p$ data and there is a difference in the $\Sigma^+ p$ channel, the difference is ascribed to the quark contribution in the $B_8 B_8$ interaction.

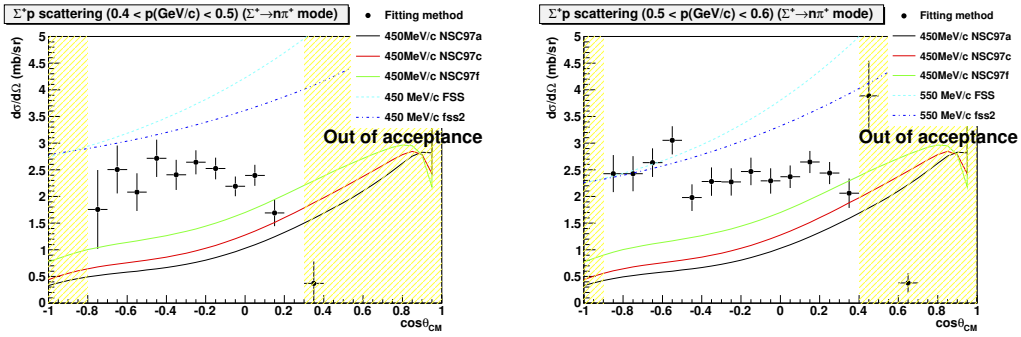

Fig. 8. Expected differential cross sections of the $\Sigma^+ p$ elastic scattering in the beam momentum regions of $0.4 < p$ (GeV/c) < 0.5 (left) and of $0.5 < p$ (GeV/c) < 0.6 (left) for the $\Sigma^+ \to n\pi^+$ decay mode which were obtained from simulated data. The assumed cross section in the simulation is 30 mb with a flat angular distribution (2.4 mb/sr). The yellow hatched region shows the region out of acceptance. Theoretical predictions by the OBEP (Nijmegen Soft Core) models and the quark cluster (RGM FSS) models are shown together.

Summary

We are proposing the Σp scattering experiment at J-PARC with 100 times larger statistics than the past experiment. The experiment will be performed at the K1.8 beam line by utilizing the K1.8 beam line spectrometer and the SKS spectrometer. A high intensity π beams of 2×10^7/spill at 1.32 GeV/c and 1.42 GeV/c for the Σ^- and Σ^+ productions, respectively, are used to produce as many hyperon beam as possible. With 16×10^6 Σ^- beam and 55×10^6 Σ^+ beam around 500 MeV/c which are tagged by the spectrometers, we will detect ~10,000 $\Sigma^- p$ and $\Sigma^+ p$ scattering events and ~6,000 $\Sigma^- p \to \Lambda n$ inelastic reaction events in 60 days beam time in total. We are now making progress on designing the detector setup and detailed simulation study.

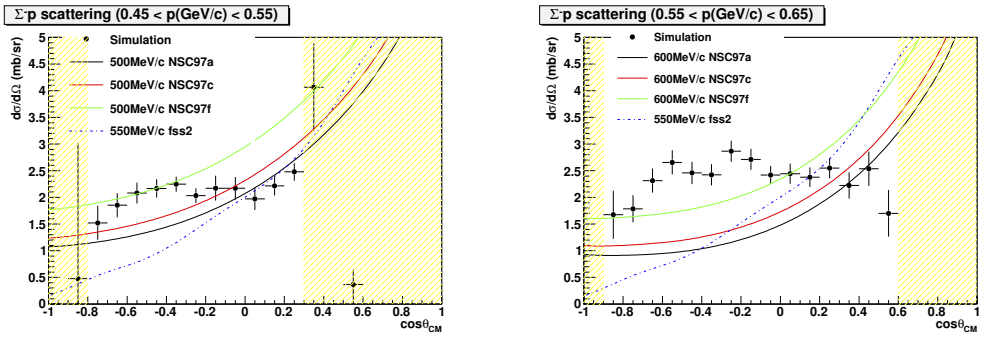

Fig. 9. The expected differential cross sections of the $\Sigma^- p$ scattering in the beam momentum regions of 0.45 $< p$ (GeV/c) < 0.55 (left) and of $0.55 < p$ (GeV/c) < 0.65 (left) which were obtained from simulated data. The differential cross section is the obtained from the integral of the Gauss peak of the $d^2\sigma/d\Omega dE$. The yellow hatched region shows the region out of acceptance. Theoretical predictions by the OBEP (Nijmegen Soft Core) models and the quark cluster (RGM FSS) models are shown together.

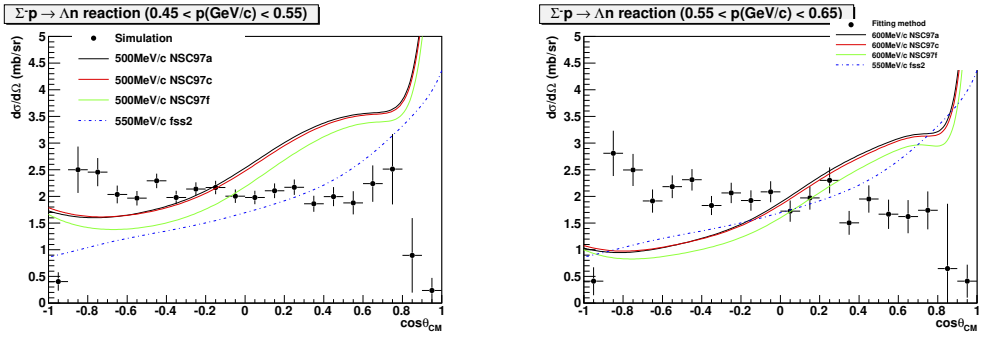

Fig. 10. Expected differential cross sections of the $\Sigma^- p \to \Lambda n$ inelastic scattering in the beam momentum regions of $0.45 < p$ (GeV/c) < 0.55 (left) and of $0.55 < p$ (GeV/c) < 0.65 (left) which were obtained from simulated data. Theoretical predictions by the OBEP (Nijmegen Soft Core) models and the quark cluster (RGM FSS) models are shown together.

Acknowledgment

We would like to express our thanks to K. Yoshimura, I. Nakamura, M. Tanaka and C.d.L. Taille for a collaboration of development of the SPIROC readout board. We acknowledge N. Chiga for his technical supports. This work was supported by dean's Grant for Exploratory Research (Graduate School of Science at Tohoku university). This work is also supported by Grant-in-Aid for Young Scientist (A) (23684011) and Scientific Research (B) (21340069).

References

1. M. M. Nagels *et al.*, Phys. Rev. D15 (1977) 2547; D20 (1979) 1633; P. M. Maessen *et al.*, Phys. Rev. C40 (1989) 2226; Th. A. Rijken *et al.*, Nucl. Phys. A547 (1992) 245c.
2. M. Oka and K. Yasaki, Quarks and Nuclei, et. W. Weise, Vol 1 (World Scientific, 1984) 489; K. Yazaki, Nucl. Phys. A479 (1988) 217c; K. Shimizu, Nucl. Phys. A547 (1992) 265c.
3. Y. Fujiwara, C. Nakamoto, Y. Suzuki, Prog. Theor. Phys. 94 (1995) 214; 94 (1995) 353; Phys. Rev. Lett. 76 (1996) 2242; Phys. Rev. C54 (1996) 2180.
4. Y. Fujiwara, Y. Suzuki, C. Nakamoto, Prog. Nucl. Part. Phys. 58 (2007) 439.

5. T. Inoue *et al.*, HAL QCD collaboration, arXiv:1007:3559 [hep-lat]
6. R. Engelmann *et al.* Phys. Lett. 21 (1966) 587; B. Sechi-Zorn *et al.* Phys. Rev. 175 (1968) 1735; G. Alexander *et al.* Phys. Rev. 173 (1968) 1452; J. A. Kadyk *et al.* Nucl. Phys. B 27 (1971) 13; F. Eisele *et al.* Phys. Lett. B 37 (1971) 204.
7. Y. Kondo *et al.* Nucl. Phys. A 676 (2000) 371
8. J.K. Ahn *et al.* Nucl. Phys. A 761 (2005) 41.
9. R. Jastrow, Phys. Rev. 81 (1950) 636.
10. http://omega.in2p3.fr/